

Materials with Hierarchical Porosity Enhance the Stability of Infused Ionic Liquid Films

Yaraset Galvan, Johannes Bauernfeind, Patrick Wolf, Ramon Zarraga, Marco Haumann, and Nicolas Vogel*



Cite This: *ACS Omega* 2021, 6, 20956–20965



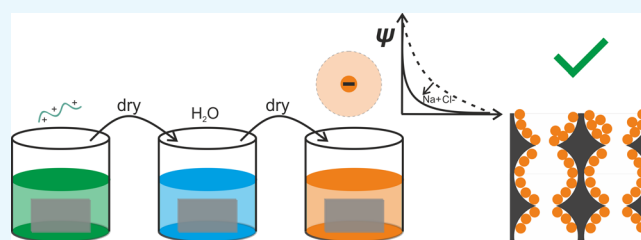
Read Online

ACCESS |

Metrics & More

Article Recommendations

ABSTRACT: Defined surface functionalities can control the properties of a material. The layer-by-layer method is an experimentally simple yet very versatile method to coat a surface with nanoscale precision. The method is widely used to either control the chemical properties of the surface via the introduction of functional moieties bound to the polymer or create nanoscale surface topographies if one polymeric species is replaced by a colloidal dispersion. Such roughness can enhance the stability of a liquid film on top of the surface by capillary adhesion. Here, we investigate whether a similar effect allows an increased retention of liquid films within a porous surface and thus potentially increases the stability of ionic liquid films infused within a porous matrix in the supported ionic liquid-phase catalysis. The complex geometry of the porous material, long diffusion pathways, and small sizes of necks connecting individual pores all contribute to difficulties to reliably coat the required porous materials. We optimize the coating process to ensure uniform surface functionalization via two steps. Diffusion limitations are overcome by force-wetting the pores, which transports the functional species convectively into the materials. Electrostatic repulsion, which can limit pore accessibility, is mitigated by the addition of electrolytes to screen charges. We introduce nanoscale topography in microscale porous SiC monoliths to enhance the retention of an ionic liquid film. We use γ - Al_2O_3 to coat monoliths and test the retention of 1-butyl-2,3-dimethylimidazolium chloride under exposure to a continuous gas stream, a setup commonly used in the water-gas shift reaction. Our study showcases that a hierarchical topography can improve the stability of impregnated ionic liquid films, with a potential advantage of improved supported ionic liquid-phase catalysis.



1. INTRODUCTION

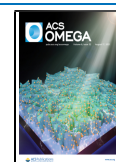
The layer-by-layer (LbL) technique is a simple yet very versatile process to introduce functional coatings with nanoscale dimensions in a wide range of materials.^{1,2} In this method, pairs of polymers with mutually attractive properties are iteratively allowed to adsorb to a surface, thus building up a coating consisting of fuzzy, alternating layers. In the simplest case, the polymeric species are oppositely charged, creating electrostatic attractions between the alternating layers. The deposition cycle can be repeated indefinitely, and because of the ionic nature of the polymers, the process is self-limiting and every immersion leads to absorption of a single layer, thus providing an excellent control over film thickness.^{2–4} In addition to electrostatic attraction, a range of other attractive interactions including hydrogen bonds,^{5,6} covalent or step-by-step reactions,⁷ host–guest interactions or biorecognition,^{8,9} and hybridization of DNA base pairs¹⁰ have been exploited to create coatings via the LbL approach.

The LbL process provides a range of attractive features: it is scalable and experimentally simple to apply, objects of any shape can be coated, provided they can be brought in contact with a liquid, and the film thickness and composition can be

readily adjusted, even at smallest length scales. In addition, a broad range of functional groups can be introduced to the coating via the polymers to tailor the resulting coating properties.^{9,11,12} Therefore, LbL has shown to be a versatile method for the formation of controlled thin films in a wide range of applications, including optics, cell surface coatings, protective coatings, catalysis, and medical devices.^{12–16}

In addition to introducing chemical functionalities to a surface, the LbL method allows the creation of nanoscale surface topographies.^{4,11,17–19} To this end, one of the polymeric species is replaced by a colloidal dispersion, which is subsequently adsorbed to build up a particulate coating held together by a polymeric “glue” provided by the oppositely charged polymer. Upon calcination, a nanoporous coating results. This process forms the basis to create structurally

Received: May 7, 2021
Accepted: July 13, 2021
Published: August 4, 2021



colored materials,¹¹ superhydrophobic coatings,⁴ or liquid-infused coatings.¹⁷ In the latter, the nanoscale topography enhances the stability of the lubricant–solid interface via the introduction of capillary forces,¹⁷ which help to mitigate the depletion of the lubricant. For example, loss of lubricant during frost formation over lubricated surfaces was lowest for substrates with the smallest interstitial space.²⁰ Enhanced capillary effects generated by nanoscale roughness or hierarchical features also improve the lubricant retention during frost formation²¹ and condensation.²²

Within the extensive field of porous materials, there are other applications that require keeping an immobilized liquid on a surface. As a particular example, the supported ionic liquid phase (SILP) catalysis²³ exploits the relatively good wettability of ionic liquids on inorganic materials to form porous phases with a thin, catalyst-containing ionic liquid film.²⁴ Based on the evidence of enhanced lubricant retention in the design of repellent surfaces, we hypothesize that the presence of nanoscale surface roughness may also stabilize the ionic liquid film within a SILP support. An increased stability of this film, in turn, would potentially reduce losses in a catalytic reactor, where a continuous gas stream is pushed through the SILP catalyst,^{25–27} and may potentially enhance the long-term stability. In addition, enhancing the lubricant/surface interactions may be the first step toward SILP operation in the liquid phase, which is currently limited by a rapid loss of the ionic liquid during operation.

In contrast to a lubricant-infused repellent coating, however, increasing the affinity of the lubricant with the underlying solid in such processes requires homogeneous functionalization of all surface regions within a three-dimensional porous material. Evidence in the literature shows that the LbL process can be used to add polyelectrolytes^{28–30} or particle layers within the surface of porous materials, such as micro- and nanopores^{31–34} with a cylindrical geometry, membranes,³⁵ fibers,³⁶ or capillaries.³⁷ Despite this body of available literature, the successful coating of porous materials is less trivial compared to flat surfaces because of the increased surface area, transport limitations, or small geometric features preventing proper access. Typically, studies in the literature either focus on very sparse particle layers^{33,35–37} (i.e., for catalysis) or require process modifications such as charge screening by the addition of salts.^{28,38,39}

As we focus on exploring the enhanced ionic liquid–support interactions in a SILP system, we set out to coat macroscopic silicon carbide specimens (approximate dimensions of 20 cm × 2.5 cm) typically used in a SILP-based water–gas shift (WGS) reaction to produce H₂ from fossil fuels.^{40,41} These support materials exhibit porosity at the micrometer scale, which is much larger than the dimensions of the nanoparticles used in this study (Ludox silica, *d* = 20 nm). As a second porous material, we therefore investigated a porous material with a much smaller pore size with dimensions in the range of the particles to be deposited. To this end, we used inverse opals as a model platform. These materials were prepared by backfilling a polymer colloidal crystal with an inorganic precursor material.^{42–44} Upon calcination, the templating particles were combusted to give rise to a well-ordered, interconnected porous structure. In our case, the pores had a dimension of 320 nm and the necks approximately 120 nm.

We found that for both types of samples, the typical coating process did not allow functionalization of the interior of the pore walls but merely created a coating on the outer surface of

the material. We therefore analyzed in detail the limiting factors preventing accurate coating in our systems and then redesigned a suitable LbL procedure according to the specific requirements of the porous materials for successful coating of the entire porous material.

2. EXPERIMENTAL METHODS

2.1. LbL Coating of Flat Surfaces. The LbL method was applied following a protocol reported in the literature.¹⁷ Silicon wafers were cleaned with ethanol and subjected to oxygen plasma treatment for 5 min to oxidize the surface and introduce negative charges. The LbL deposition was performed by immersion of the substrates in a 0.1% w/w solution of poly(diallyldimethylammonium) chloride (PDADMAC) for 10 min followed by rinsing in deionized (DI) water. A second immersion was performed in a 0.1% w/w solution of Ludox silica particles (diameter: 20 nm) for 10 min followed by rinsing in water. The cycle was repeated five times to deposit several layers. PDADMAC was removed by combustion at 500 °C for 2 h with a 5 h ramp time.

2.2. LbL Coating of Microscale Porous Materials. Silicon carbide (SiC) monoliths with an average pore size of 3 μm were activated with oxygen plasma for 5 min. The LbL deposition was performed similarly to the coating of flat surfaces, with an additional drying step between each immersion. The first immersion used a 0.1% w/w solution of PDADMAC for 10 min followed by rinsing in DI water and drying with nitrogen. The second immersion step used a 0.1% w/w dispersion of Ludox silica particles for 10 min followed by rinsing in water and drying with nitrogen. The cycle was repeated five times, and PDADMAC was removed by combustion at 500 °C for 2 h with a 5 h ramp time.

For infusion of the ionic liquid (IL) and the leaching test, the coating solutions were exchanged as follows: after activation of SiC monoliths with plasma, the first immersion was in a 0.1% w/w dispersion of Al₂O₃ (average size: 50 nm, Alfa Aesar), which has a zeta potential of 35 mV; this gave a stable dispersion of positively charged particles. After the rinsing and drying steps, the second immersion was in a 0.1% w/w solution of poly(sodium 4-styrenesulfonate) (PSS). We coated SiC monoliths in 5, 10, and 15 cycles. The PSS was removed by combustion at 500 °C for 2 h.

2.3. Fabrication of Inverse Opals. The inverse opals were prepared following a protocol reported in the literature.⁴⁵ A solution of ethanol, tetraethyl orthosilicate (TEOS), and hydrochloric acid (0.1 M) (1.5:1:1 by weight) was stirred for 1 h in order to prehydrolyze TEOS. A monodisperse suspension (60 mL) of colloidal polystyrene (0.1% w/v, diameter: 320 nm) and prehydrolyzed TEOS solution (375 μL) was mixed and poured in 12 mL vials. Substrates cleaned by ultrasonication in ethanol and oxygen plasma treatment were vertically suspended in the vials containing the colloid/TEOS suspension. The water was slowly evaporated in an oven at 65 °C to form a thin film on the surface of the substrate. Then, the substrates were calcined at 500 °C for 2 h with a 5 h ramp time to remove the polystyrene particles and sinter the SiO₂ structure to form the inverse opals.

2.4. Coating Nanoscale Porous Materials (Inverse Opals). The inverse opals were activated with oxygen plasma for 5 min. The LbL deposition was performed similar to the coating of microscale porous materials but using solutions containing NaCl. The first immersion was into a 0.1% w/w solution of PDADMAC with NaCl (1, 10, 30, 50, and 100

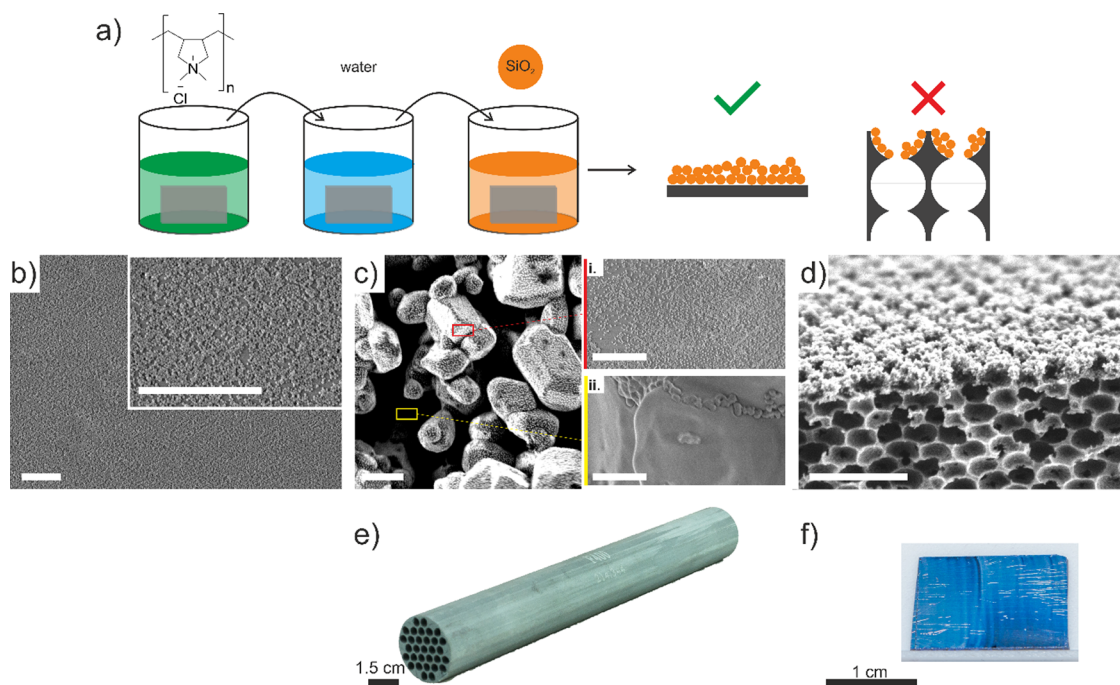


Figure 1. LbL coating of different surfaces by SiO_2 particles. (a) Schematic representation of the LbL process that consists of immersion of a substrate (flat or porous) in the positively charged PDADMAC followed by rinsing in water to get rid of excess of polymer and then in a solution of negatively charged SiO_2 particles. A homogenous coating is obtained on flat surfaces, but in the porous material, the particles do not form a coating in the inner pores. Resulting coating on (b) a flat Si wafer and (c) a porous SiC ($3 \mu\text{m}$ average pore size) monolith (i) magnification of the outer surface of the SiC monolith and (ii) magnification of the inner pore of the SiC monolith. (d) Resulting coating of SiO_2 inverse opals (350 nm average pore size). All scale bars of (b–d) equal $1 \mu\text{m}$. Photograph of (e) SiC monolith and (f) inverse opal in a Si wafer.

mM) for 10 min followed by rinsing in DI water and drying with N_2 . The second immersion was into a 0.1% w/w solution of Ludox silica particles with NaCl (1, 10, 30, 50, and 100 mM) for 10 min followed by rinsing in water and drying with N_2 . The cycle was repeated five times, and PDADMAC was removed by combustion at $500 \text{ }^\circ\text{C}$ for 2 h with a 5 h ramp time.

2.5. Infusion of IL in SiC Monoliths. Before infusing the SiC monoliths, both the monoliths and the IL were dried. 1-Butyl-2,3-dimethylimidazolium chloride [BMMIM][Cl] (99%, solvent innovation) was placed in a desiccator together with the silica gel in vacuum for 24 h. The SiC monoliths were dried at $110 \text{ }^\circ\text{C}$ for 2 h just before the infusion. A 10% v/v solution of dried [BMMIM][Cl] in dichloromethane was prepared. The SiC monoliths were immersed in the solution for 5 min and dried under vacuum for 24 h.

2.6. Leaching Test of SiC Monoliths. [BMMIM][Cl]-infused SiC monoliths were weighed before and after every 5 h of compressed air streaming. Noncoated and coated monoliths with 5, 10, and 15 coating cycles were compared.

2.7. Scanning Electron Microscopy (SEM). A Zeiss Gemini 500 SEM was used. Silicon wafer substrates coated with a nanoparticle layer were used without further modification. SiC monoliths were carefully broken to observe the inner pores after coating. Cross-sectional samples of inverse opals were fabricated by breaking the substrate along the crystal plane of the wafer using a diamond cutter only in the corners.

2.8. Zeta Potential. Zeta potential measurements were performed with a Zetasizer Nano ZS, Malvern Instruments. All samples were dispersed in a glass cuvette at a particle

concentration of 0.1 wt % and varying concentrations of NaCl (0, 1, 10, 30, 50, and 100 mM).

2.9. Physisorption Analysis (Brunauer–Emmett–Teller (BET) Surface Area). BET surface areas were measured by gas sorption analysis with nitrogen using a Nova, Quantachrome. The samples were ground into pieces smaller than 5 mm. The pulverized samples (0.4 g) were analyzed in each measurement.

3. RESULTS AND DISCUSSION

We employ the LbL process to create layers of SiO_2 nanoparticles to enhance the nanoporosity of a surface.^{4,17–19} To this end, we created negative charges on the surface by means of plasma treatment. Subsequently, the substrate was immersed in a 0.1% w/w solution of PDADMAC as a positively charged polyelectrolyte. Then, the sample was rinsed with water and immersed in a 0.1% w/w solution of Ludox silica colloidal particles (see Figure 1(a)). These steps were then iterated to create a coating. After having completed five cycles, the surface was calcined to completely remove the organic components and leave a particulate coating on the surface. Figure 1(b) shows a planar silicon wafer successfully coated with five layers of 20 nm SiO_2 .

When coating a porous material with SiO_2 following the same procedure, the coating was exclusively deposited at the outer surface of the material, whereas the inner pores remained uncoated. The failure to coat the porous material persisted for materials with different pore sizes. We first tried to coat SiC monoliths with an average pore size of $3 \mu\text{m}$ as shown in Figure 1(c) as an example of a material with a large porosity. Such monoliths find applications in the SILP-catalyzed WGS and hydroformylation reactions.^{41,46} The top SEM image (i)

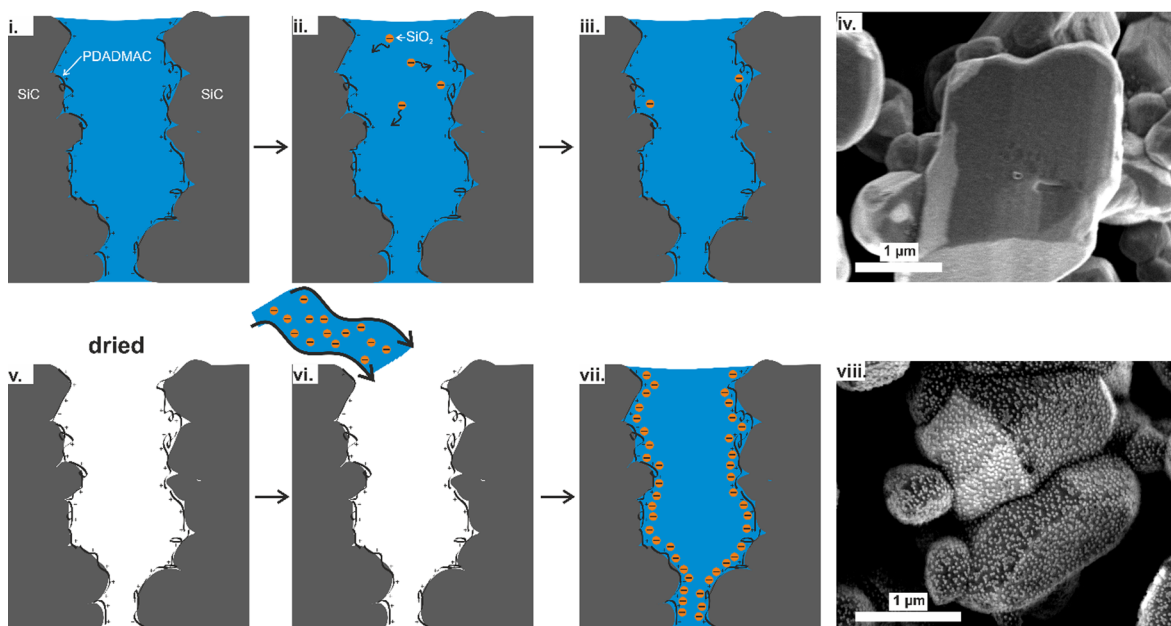


Figure 2. SiC monolith with micrometer-scale porosity coated with SiO₂ particles via the LbL technique. Schematic representation of the LbL coating process in two different scenarios. The top part depicts the conventional LbL process, while the bottom part shows the modified process with an intermediate drying step in between each immersion. Panel (i) shows an inner pore immersed in PDADMAC solution, panel (ii) depicts the diffusion of SiO₂ particles inside a pore flooded from the previous coating step, panel (iii) shows the unsuccessful SiO₂ coating with the conventional coating process, and panel (iv) shows a representative SEM image of the surface of an actual pore in a SiC monolith unsuccessfully coated. The bottom row shows the modified process. Panel (v) shows a dried inner pore coated with a layer of PDADMAC, panel (vi) shows the introduction of the SiO₂ dispersion by convective wetting into a dry pore, which created a uniform concentration profile and thus achieves a homogeneous coating (vii). Panel (viii) shows a representative SEM image of a successfully coated pore.

shows a high magnification image of the outer surface, which was successfully coated with the SiO₂ particles. The bottom image (ii) shows an inner section of the same monolith after breaking and shows a pristine, uncoated surface.

Similarly, an inverse opal coated with the same procedure was only functionalized at the top layer (Figure 1(d)). This structure was formed using an evaporative coassembly approach, where colloidal particles formed a periodic structure by convective assembly.⁴⁵ Tetraethylorthosilicate as a silica precursor was added to the reaction mixture and deposited in the interstitial sites. Upon calcination, the inverse replica of the colloidal crystal was formed, exhibiting a regular, interconnected porosity with an average pore diameter of 320 nm.

To address the limitations of the LbL technique in coating porous materials, we first investigated several parameters during the coating of the SiC monoliths with micrometer-scale porosity that may be affected by the nature of the porous materials. As mentioned above, prior to the actual LbL process, it is necessary to activate the surface to introduce negatively charged hydroxyl groups via oxygen plasma.¹⁷ Here, taking into account the tortuosity of the porous network, we increased the treatment time to allow the plasma to diffuse further into the porous network. Second, we considered the increased surface area in porous materials and increased the concentration in both coating solutions to ensure that all available surfaces can be coated. A successfully coated flat surface needs only 0.1 wt % solutions of either PDADMAC or colloidal SiO₂.¹⁷ For the porous SiC, we increased the concentration to 1 wt %. Third, we increased the immersion time of the porous materials in the different coating solutions. Since the pores are filled with water, after each rinsing step before immersion into the coating solutions, either type of surface functionality to be attached

needs to diffuse into the porous system to coat the surface. This diffusion time to reach the surface is greatly increased compared to a flat surface. We therefore increased the immersion time from 5 min used for flat surfaces to 60 min for the porous surfaces.

We adapted the oxygen plasma treatment, the concentration of the coating solutions, and the immersion times, first separately, and in a second attempt, together. Even after implementation of the three different aspects simultaneously, the inner surface of the porous material was not coated. Since there was a slight increase in the coating depth with increasing time, we inferred that diffusion of PDADMAC and SiO₂ into the pores is the limiting step preventing efficient pore functionalization. The difficulties in coating the porous SiC monolith were surprising, given the large pore sizes in the material (Figure 1) and the body of literature suggesting successful LbL coatings on porous materials.^{31–34} Seemingly, and in contrast to typical porous materials used in the literature, the macroscopic dimensions (pore diameter = 3 μm) of the monolith lead to transport limitations for the ionic species involved in the LbL process.

Next, we therefore implemented an additional step to circumvent the slow diffusion process of the particles and polymer chains into the liquid-filled porous material. After each immersion of the porous material in the coating solutions, we rinsed it in water and subsequently dried the entire sample with a flow of nitrogen. In this way, when the porous material is immersed into the next coating solution, either PDADMAC or the SiO₂ particles are dragged along with the liquid filling the pores. The coating process therefore becomes independent of the diffusion limitations.

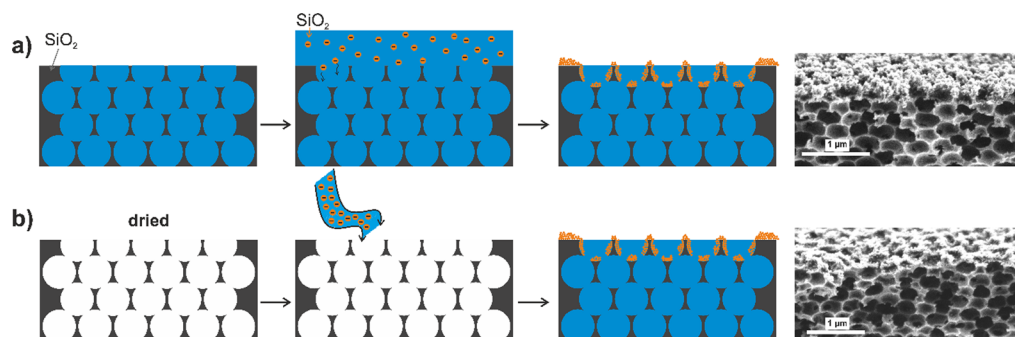


Figure 3. Inverse opals coated with SiO₂ nanoparticles (20 nm) using the conventional LbL technique (a) and the modified LbL version with a convective flow of solutions of PDADMAC and SiO₂ colloidal particles (b).

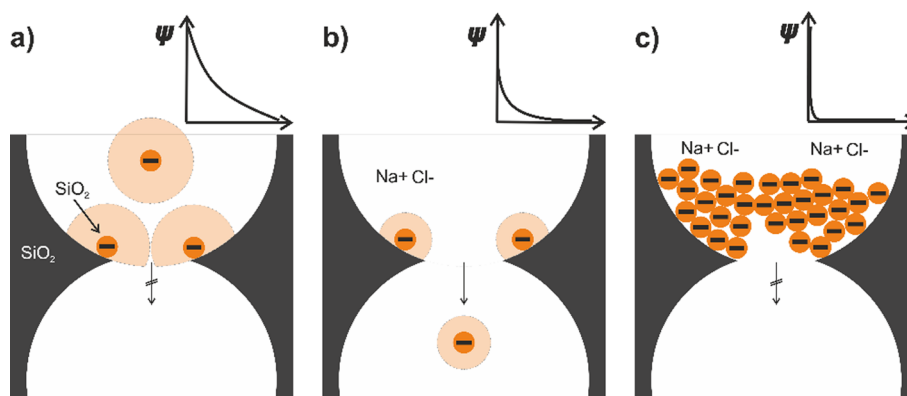


Figure 4. Schematic illustration of the effect of the surface potential of adsorbed particles on pore accessibility. Three possible scenarios at the neck of two pores of an inverse opal are compared. (a) The surface potential of two adsorbed particles extends into the neck region and therefore restricts pore accessibility of like-charged particles. (b) With the addition of salt, the electrostatic double layer is screened, providing pore access for a like-charged particle. (c) At a high salt concentration, the charge screening becomes pronounced enough to compromise the colloidal stability, leading to adsorption of particle agglomerates, which physically block the pore.

Figure 2 schematically shows the difference in the coating process, illustrating the concentration profile of a species to be coated (i.e., the silica particles) within a single pore. The top part (i–iii) shows the conventional LbL process without the intermediate drying step. The SiO₂ particles enter the pores from the top. Due to the slow diffusion and continuous adsorption to the wall, the concentration decreases toward the interior of the pore. Figure 2(iv) shows the absence of any coated SiO₂ particles on the surface of an inner pore treated using this process. The bottom part (Figure 2(v–vii)) shows the coating process with the intermediate drying step in between each immersion. The dispersed SiO₂ particles are dragged into the porous network by a convective flow and maintain a high concentration. This process modification allowed reliable coating of the inner pore walls of the SiC monolith, as shown in the SEM image of Figure 2(viii).

Next, we investigated the coating of the interior pore walls of an inverse opal, which has an interconnected porous network with pore dimensions of around 320 nm.

Figure 3 shows a schematic illustration of the coating strategies to coat the pores of an inverse opal, following the conventional LbL approach (Figure 3(a)). As expected, the side-view SEM image showed that only the outermost pore layer was coated with silica nanoparticles. Similar to the case of the porous monolith, we first hypothesized that the 20 nm SiO₂ particles were not able to coat the inner pores because of two reasons: the necks in the first row of pores are potentially clogged with PDADMAC and SiO₂ that attract each other and

the diffusion limitations,^{47,48} which are even more pronounced because of the considerably smaller pores and the necks that connect them. We then applied the developed coating strategy toward the inverse opals in which we capitalize on convection to enhance the mass transport of colloidal particles into the pore network (Figure 3(b)). We used the structural coloration of the inverse opal to monitor the process steps.^{18,42,49,50} Successful drying of the pores in between the deposition steps could be seen by the presence of structural color, which is caused by the high refractive index contrast between silica matrix and air. In contrast, after immersion, the water-filled pores exhibit a much lower refractive index contrast and thus lose their coloration.^{18,50} Even though this structural color-based monitoring indicated that the entire porous network was dried in between all immersion steps, the developed methodology did not lead to a coating of the inner pore walls. Similar to the abovementioned case, the side-view SEM image showed that only the uppermost row of the inverse opal was decorated with silica nanoparticles. Even though the SiO₂ particles ($d = 20$ nm) were notably smaller than the necks of the pores ($d = 119 \pm 13$ nm), the particles apparently could not be transported through the pore network.

Based on reports in the literature that the addition of salt can facilitate the coating efficiency in confinements,^{28,29,51} we hypothesize that the inability of the colloidal SiO₂ to penetrate through the pore network may be related to the electrostatic properties of the colloids in our system as well. The potential of a charged surface penetrates into an electrolyte solution and

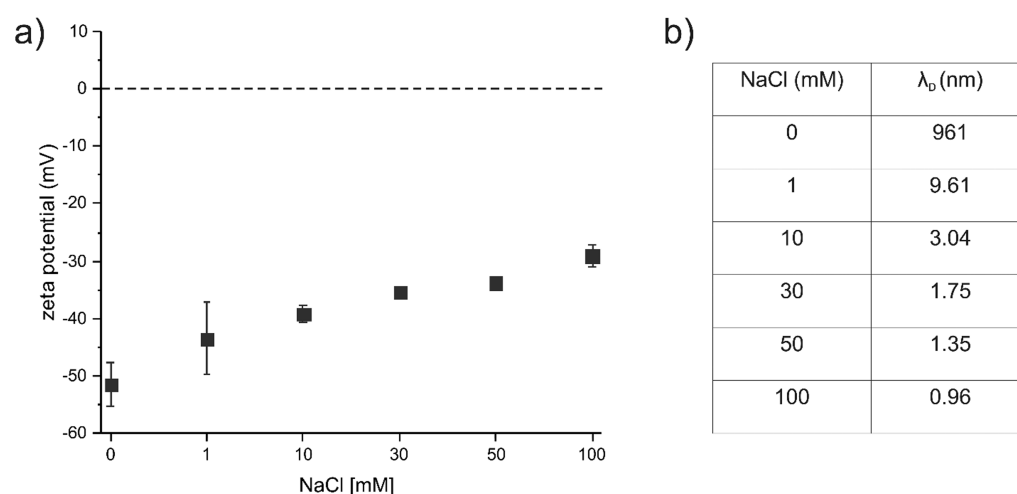


Figure 5. (a) Zeta potential of the colloidal SiO₂ in dispersions with different concentrations of NaCl. (b) Debye length in solutions with different concentrations of NaCl.

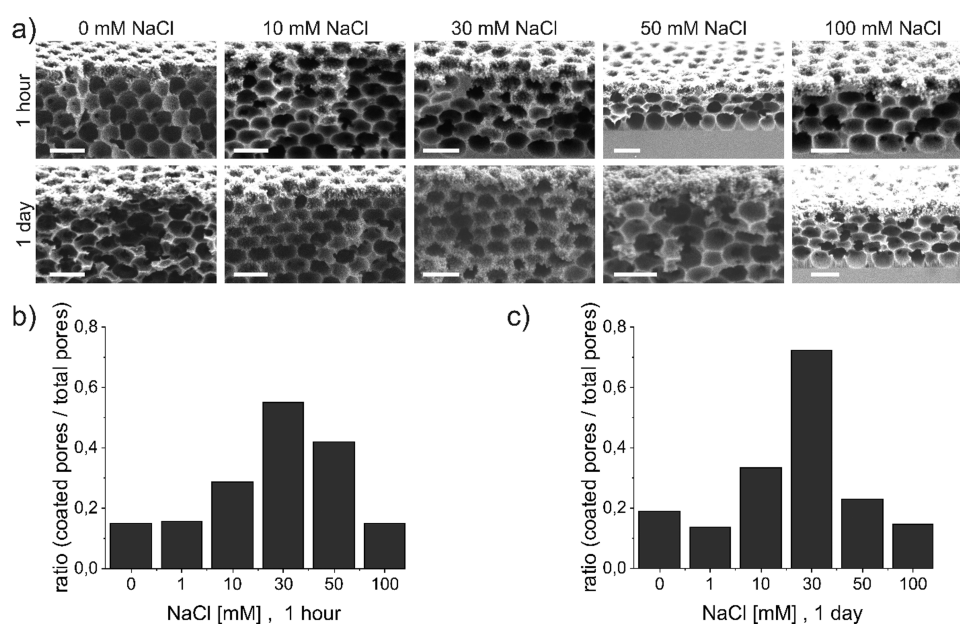


Figure 6. Influence of salt concentration on the pore functionalization efficiency of inverse opals coated using the LbL method. (a) Representative side-view SEM images of inverse opals coated using the LbL technique with dispersions of colloidal SiO₂ with different NaCl concentrations (columns) and different immersion times (rows), scale bars: 500 nm. (b, c) Statistical analysis of the pore functionalization efficiency showing the ratio of coated pores as a function of salt concentration for immersion times of 1 h (b) and 1 day (c). Over 500 pores were analyzed for each experiment.

decays as counterions accumulating around the surface. The extent of this penetration is described by the Debye length, defined as the distance from the surface when the electrostatic potential drops to $1/e$.⁵² The decay of the potential is therefore determined by the ion concentration in the solution.⁵² We hypothesize that the electrostatic repulsion blocks pore access of the silica particles as schematically illustrated in Figure 4. During the LbL process, electrostatic adsorption of silica particles will take place at the outer layer of the porous surface upon contact, leading to particles being deposited close to the pore opening as well. The surface potential of these adsorbed silica particles, in turn, will extend into the neck region, effectively reducing the available opening for an additional, like-charged silica particle to pass through (Figure 4(a)). Since the surface potential can be screened by charges,⁵² the addition of salt should decrease the Debye length,⁵² and thereby

effectively increase the accessible pore area for a like-charged particle (Figure 4(b)). With the increasing salt concentration, however, the electrostatic repulsion of the colloidal silica dispersion itself will be affected, leading to an onset of agglomeration. Such agglomerated particles are larger in size and when adsorbed onto the outer layer of the inverse opal, they physically block pore access by covering the neck (Figure 4(c)).

To test this hypothesis, we carried out a parametric study on the influence of NaCl addition on the colloidal stability and the coating of inverse opals using the LbL technique. We prepared 0.1 wt % solutions of colloidal SiO₂ with 1, 10, 30, 50, and 100 mM NaCl. We determined the zeta potential of the different SiO₂ dispersions as a function of salt concentration (Figure 5). As expected, the zeta potential decreased with the increasing

salt concentration, indicating an increased screening of charges and thus a decrease in the range of the surface potential.⁵³

Next, we tested the effect of the screened electrostatic repulsion on pore accessibility (Figure 6). To this end, we used our modified LbL process. After activation with oxygen plasma, we immersed the inverse opal in a solution of positively charged PDADMAC (0.1 wt %) with different NaCl concentrations. We then rinsed the inverse opal thoroughly with water and dried it completely using nitrogen gas. Subsequently, we immersed the sample in a dispersion of negatively charged colloidal SiO₂ (0.1 wt %) with different NaCl concentrations. In addition to the varying salt concentration, we also varied the exposure time to account for the slow diffusion within the porous network and exposed the inverse opals to individual solutions for 1 h and 1 day, respectively.

Figure 6(a) shows the representative side-view SEM images of the different inverse opal samples coated using the LbL technique with coating solutions containing different salt concentrations and using the two immersion times. All samples were coated with three layers using the previously described procedure, calcined to remove the organic PDADMAC polymer, and broken into two parts to reveal the pore interior in the side-view images. Using image analysis, we determined the fraction of functionalized pores for the different samples by counting around 500 pores per sample (Figure 6(b,c)).

Without the addition of NaCl, no particles were deposited in the interior pores, even for the extremely long immersion time of 1 day, corroborating the inability of the particle to access the pores. In contrast, the addition of 10 mM NaCl allowed at least some silica particles to enter the porous network. For both immersion times, we determined around 30% of the inner pores coated. It is worth noting that at this salt concentration, the extent of the surface potential surrounding the particle, characterized by the Debye length (Figure 5(b)), is already significantly smaller than the average neck size ($d = 119 \pm 13$ nm), indicating that particles can already pass through the opening. However, seemingly, the likelihood of diffusing particles to penetrate the necks is not yet sufficient to reliably coat the porous material. Using coating solutions with 30 mM NaCl, we observed an increased pore coverage. Using a 1 h deposition time, around 50% of all pores were coated. With an immersion time of 1 day, the fraction of the coated pores increased to 70%, indicating that the charge screening indeed increased the pore accessibility. With the increasing salt concentration (50 mM), the fraction of coated pores was reduced again, which we interpret as an onset of agglomeration that hinders pore access. For a salt concentration of 100 mM, no particles were detected in the pore interior and a close inspection of the surface structure revealed the presence of agglomerates deposited on the topmost layer. Apparently, a salt concentration of 30 mM provides a compromise between sufficient colloidal stability and decreased Debye length, which optimizes pore accessibility.

Having established a reliable protocol to introduce a nanoscale topography in our porous materials, we tested its effect on the stability and retention of an infused IL film. Based on the fact that a liquid film can be efficiently infused into nanoporous coatings on flat surfaces to design liquid-repellent surfaces,¹⁸ we aimed to transfer this concept to a porous material. We used the SiC monoliths with hierarchical porosity and infused a layer of [BMMIM][Cl] as the IL. This combination of support and IL is of interest in catalytic

applications, for example, for a SILP-based WGS reaction to produce H₂ from fossil fuels.^{54–56} In this SILP approach, a thin layer of IL is confined in the pores of a porous material, such as the SiC monoliths. This SILP further contains a dissolved molecular catalyst and combines the high surface area and ease of operation of heterogeneous catalysis with the selectivity of a homogeneous catalyst.^{23,26,57,58}

Recent studies showed that aluminum oxide (γ -Al₂O₃) is an ideal support for the IL and the catalyst for the WGS reaction.^{41,59} Here, we investigated whether nanoscale alumina particles can be coated onto the porous SiC monolith to create additional capillary forces acting through the nanoscale porosity. With the coating, we anticipate a more stable confinement of the IL within the SiC monolith. We subjected the SiC monolith to our modified LbL protocol using a dispersion of positively charged γ -Al₂O₃ particles (50 nm, 0.1 wt %) and negatively charged PSS (0.1 wt %). The SiC monoliths have a surface area of 0.2 m²/g (LiqTech International A/S). After five layers of coating, the SiC monolith had a relative surface area of 1.43 m²/g and with 15 layers of coating, it had a relative surface area of 2.9 m²/g, such areas were obtained using N₂ physisorption, which indicates a nonlinear increment of the surface area as a function of the deposited layers of γ -Al₂O₃. Figure 7(a–c) shows the interior of a monolith successfully coated with γ -Al₂O₃ nanoparticles at different magnifications.

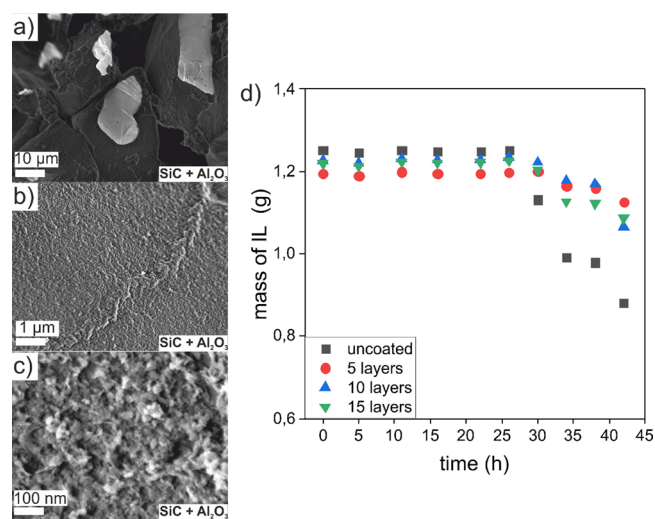


Figure 7. Enhanced retention of IL films by nanoscale surface roughness within a porous material. (a–c) SEM images of the inner pores of a SiC monolith coated with 15 layers of γ -Al₂O₃ nanoparticles using the LbL method with a convective flow of coating solutions. (d) Gravimetric evaluation of the retention of the IL in coated and noncoated SiC monoliths.

Finally, we compared the retention of the IL film infiltrated in pristine and γ -Al₂O₃ nanoparticle-coated SiC monoliths. To this end, we immersed the monoliths into 10 v/v% solution of [BMMIM][Cl] in dichloromethane (DCM) and evaporated the DCM to leave an impregnated IL film within the solid support.⁴¹

We simulated the reaction conditions occurring in a continuous gas-phase flow reactor by streaming a current of compressed air through the monoliths. We evaluated the IL retention by gravimetrically determining the loss of IL over time (Figure 7(d)). All coated samples consistently showed a

lower IL loss compared to the uncoated reference. After 42 h, only 70% of the initial IL was retained in the reference sample, while the coated monoliths held between 90 and 95% of the initial IL. The loss of IL in this simulated reactor setup could thus be decreased by a factor of 6, underlining the potential of employing capillary forces by nanoscale surface roughness.

4. CONCLUSIONS

The LbL process is a simple yet powerful technique to create defined surface coatings for a broad range of applications. Here, we demonstrate that a nanoscale topography can enhance the stability of an IL film infused in a porous solid support. We first explore strategies to successfully coat the inner pore walls of our porous materials of interest. We realize that a combination of transport limitations and pore accessibility is the main limitation hindering the coating process. We overcome this limitation via two modifications of the coating process. First, adding convective flows by intermediate drying steps overcomes diffusive transport limitations and allows coating of porous materials with micrometer-scale porosity. Second, screening electrostatic repulsion effects by the addition of salt overcomes the limited accessibility for pores in the nanometer range.

In a proof of principle, we show how nanoscale surface roughness created by LbL deposition of γ - Al_2O_3 nanoparticles within a porous monolith can enhance capillary interactions and thus increases the retention of an IL film infused into the porous material.

AUTHOR INFORMATION

Corresponding Author

Nicolas Vogel – Institute of Particle Technology, Friedrich-Alexander University Erlangen-Nürnberg, 91058 Erlangen, Germany; orcid.org/0000-0002-9831-6905; Email: nicolas.vogel@fau.de

Authors

Yaraset Galvan – Institute of Particle Technology, Friedrich-Alexander University Erlangen-Nürnberg, 91058 Erlangen, Germany; Departamento de Química, División de Ciencias Naturales y Exactas, Universidad de Guanajuato, 36050 Guanajuato, Mexico

Johannes Bauernfeind – Institute of Particle Technology, Friedrich-Alexander University Erlangen-Nürnberg, 91058 Erlangen, Germany

Patrick Wolf – Lehrstuhl für Chemische Reaktionstechnik (CRT), Friedrich-Alexander-Universität Erlangen-Nürnberg (FAU), 91058 Erlangen, Germany

Ramon Zarraga – Departamento de Química, División de Ciencias Naturales y Exactas, Universidad de Guanajuato, 36050 Guanajuato, Mexico

Marco Haumann – Lehrstuhl für Chemische Reaktionstechnik (CRT), Friedrich-Alexander-Universität Erlangen-Nürnberg (FAU), 91058 Erlangen, Germany; orcid.org/0000-0002-3896-365X

Complete contact information is available at:

<https://pubs.acs.org/10.1021/acsomega.1c02405>

Author Contributions

N.V. and Y.G. conceived the study. Y.G. performed the synthesis of inverse opals, the surface functionalization of inverse opals, and zeta potential characterization. J.B. coated SiC monoliths and performed the leaching test. J.B. and P.W.

discussed the leaching test. M.H., J.B., Y.G., and N.V. discussed the strategies for coating the porous materials. N.V., M.H., and R.Z. supervised the research. The manuscript was written through contributions of Y.G. and N.V. All authors have given approval to the final version of the manuscript.

Funding

This project was supported by the Deutsche Forschungsgemeinschaft (DFG) under grant number VO1824/9-1. Y.G. and N.V. acknowledge funding from the women representatives at the Faculty of Engineering. N.V. and M.H. also acknowledge funding of the DFG via the collaborative research center “catalysis at liquid interfaces” (SFB 1452). N.V. acknowledges support of the Interdisciplinary Center for Functional Particle System (FPS) at FAU Erlangen.

Notes

The authors declare no competing financial interest.

REFERENCES

- (1) Decher, G.; Hong, J. D. Buildup Of Ultrathin Multilayer Films By A Self-Assembly Process .1. Consecutive Adsorption Of Anionic And Cationic Bipolar Amphiphiles On Charged Surfaces. *Makromol. Chemie-Macromolecular Symp.* **1991**, *46*, 321–327.
- (2) Decher, G. Fuzzy Nanoassemblies: Toward Layered Polymeric Multicomposites. *Science* **1997**, *277*, 1232–1237.
- (3) Fou, A. C.; Rubner, M. F. Molecular-Level Processing Of Conjugated Polymers. 2. Layer-By-Layer Manipulation Of In-Situ Polymerized P-Type Doped Conducting Polymers. *Macromolecules* **1995**, *28*, 7115–7120.
- (4) Bravo, J.; Zhai, L.; Wu, Z.; Cohen, R. E.; Rubner, M. F. Transparent Superhydrophobic Films Based On Silica Nanoparticles. *Langmuir* **2007**, *23*, 7293–7298.
- (5) Kim, B. S.; Lee, H. I.; Min, Y.; Poon, Z.; Hammond, P. T. Hydrogen-Bonded Multilayer Of PH-Responsive Polymeric Micelles With Tannic Acid For Surface Drug Delivery. *Chem. Commun.* **2009**, 4194–4196.
- (6) Hammond, P. T. Building Biomedical Materials Layer-By-Layer. *Mater. Today* **2012**, *15*, 196–206.
- (7) Such, G. K.; Quinn, J. F.; Tjipto, E.; Caruso, F. Assembly Of Ultrathin Polymer Multilayer Films By Click Chemistry. *J. Am. Chem. Soc.* **2006**, *128*, 9318–9319.
- (8) Muller, W.; Ringsdorf, H.; Rump, E.; Wildburg, G.; Zhang, X.; Angermaier, L.; Knoll, W.; Liley, M.; Spinke, J. Attempts To Mimic Docking Processes Of The Immune System: Recognition-Induced Formation Of Protein Multilayers. *Science* **1993**, *262*, 1706–1708.
- (9) Mansouri, S.; Merhi, Y.; Winnik, F. M.; Tabrizian, M. Investigation Of Layer-By-Layer Assembly Of Polyelectrolytes On Fully Functional Human Red Blood Cells In Suspension For Attenuated Immune Response. *Biomacromolecules* **2011**, *12*, 585–592.
- (10) Johnston, A. P. R.; Read, E. S.; Caruso, F. DNA Multilayer Films On Planar And Colloidal Supports: Sequential Assembly Of Like-Charged Polyelectrolytes. *Nano Lett.* **2005**, *5*, 953–956.
- (11) Wang, C. X.; Braendle, A.; Menyo, M. S.; Pester, C. W.; Perl, E. E.; Arias, I.; Hawker, C. J.; Klinger, D. Catechol-Based Layer-By-Layer Assembly Of Composite Coatings: A Versatile Platform To Hierarchical Nano-Materials. *Soft Matter* **2015**, *11*, 6173–6178.
- (12) Zhao, S.; Caruso, F.; Dahne, L.; Decher, G.; De Geest, B. G.; Fan, J.; Feliu, N.; Gogotsi, Y.; Hammond, P. T.; Hersam, M. C.; Khademhosseini, A.; Kotov, N.; Loporatti, S.; Li, Y.; Lisdat, F.; Liz-Marzan, L. M.; Moya, S.; Mulvaney, P.; Rogach, A. L.; Roy, S.; Shchukin, D. G.; Skirtach, A. G.; Stevens, M. M.; Sukhorukov, G. B.; Weiss, P. S.; Yue, Z.; Zhu, D.; Parak, W. J. The Future Of Layer-By-Layer Assembly: A Tribute To ACS Nano Associate Editor Helmut Mohwald. *ACS Nano* **2019**, *13*, 6151–6169.
- (13) Kujawa, P.; Schmauch, G.; Viitala, T.; Badia, A.; Winnik, F. M. Construction Of Viscoelastic Biocompatible Films Via The Layer-By-Layer Assembly Of Hyaluronan And Phosphorylcholine-Modified Chitosan. *Biomacromolecules* **2007**, *8*, 3169–3176.

- (14) Szweda, R.; Tschopp, M.; Felix, O.; Decher, G.; Lutz, J. F. Sequences Of Sequences: Spatial Organization Of Coded Matter Through Layer-By-Layer Assembly Of Digital Polymers. *Angew. Chem. Int. Ed.* **2018**, *57*, 15817–15821.
- (15) Escobar, A.; Muzzio, N.; Moya, S. E. Antibacterial Layer-By-Layer Coatings For Medical Implants. *Pharmaceutics* **2021**, *13*, 16.
- (16) Motay, M.; Martel, D.; Vileno, B.; Soraru, C.; Ploux, L.; Méndez-Medrano, M. G.; Colbeau-Justin, C.; Decher, G.; Keller, N. Virtually Transparent TiO₂/Polyelectrolyte Thin Multilayer Films As High-Efficiency Nanoporous Photocatalytic Coatings For Breaking Down Formic Acid And For Escherichia Coli Removal. *ACS Appl. Mater. Interfaces* **2020**, *12*, 55766–55781.
- (17) Sunny, S.; Vogel, N.; Howell, C.; Vu, T. L.; Aizenberg, J. Lubricant-Infused Nanoparticulate Coatings Assembled By Layer-By-Layer Deposition. *Adv. Funct. Mater.* **2014**, *24*, 6658–6667.
- (18) Galvan, Y.; Phillips, K. R.; Haumann, M.; Wasserscheid, P.; Zarraga, R.; Vogel, N. Ionic-Liquid-Infused Nanostructures As Repellent Surfaces. *Langmuir* **2018**, *34*, 6894–6902.
- (19) Taketa, T. B.; Rocha Neto, J. B. M.; Dos Santos, D. M.; Fiamingo, A.; Beppu, M. M.; Campana-Filho, S. P.; Cohen, R. E.; Rubner, M. F. Tracking Sulfonated Polystyrene Diffusion In A Chitosan/Carboxymethyl Cellulose Layer-By-Layer Film: Exploring The Internal Architecture Of Nanocoatings. *Langmuir* **2020**, *36*, 4985–4994.
- (20) Rykaczewski, K.; Anand, S.; Subramanyam, S. B.; Varanasi, K. K. Mechanism Of Frost Formation On Lubricant-Impregnated Surfaces. *Langmuir* **2013**, *29*, 5230–5238.
- (21) Wong, W. S. Y.; Hegner, K. I.; Donadei, V.; Hauer, L.; Naga, A.; Vollmer, D. Capillary Balancing: Designing Frost-Resistant Lubricant-Infused Surfaces. *Nano Lett.* **2020**, *20*, 8508–8515.
- (22) Adera, S.; Alvarenga, J.; Shneidman, A. V.; Zhang, C. T.; Davitt, A.; Aizenberg, J. Depletion Of Lubricant From Nanostructured Oil-Infused Surfaces By Pendant Condensate Droplets. *ACS Nano* **2020**, *14*, 8024–8035.
- (23) Riisager, A.; Fehrmann, R.; Haumann, M.; Wasserscheid, P. Supported Ionic Liquids: Versatile Reaction And Separation Media. *Top. Catal.* **2006**, *40*, 91–102.
- (24) Öchsner, E.; Schneider, M. J.; Meyer, C.; Haumann, M.; Wasserscheid, P. Challenging The Scope Of Continuous, Gas-Phase Reactions With Supported Ionic Liquid Phase (SILP) Catalysts - Asymmetric Hydrogenation Of Methyl Acetoacetate. *Appl. Catal. Gen.* **2011**, *399*, 35–41.
- (25) Ruta, M.; Yuranov, I.; Dyson, P. J.; Laurenczy, G.; Kiwi-Minsker, L. Structured Fiber Supports For Ionic Liquid-Phase Catalysis Used In Gas-Phase Continuous Hydrogenation. *J. Catal.* **2007**, *247*, 269–276.
- (26) Riisager, A.; Fehrmann, R.; Flicker, S.; Van Hal, R.; Haumann, M.; Wasserscheid, P. Very Stable And Highly Regioselective Supported Ionic-Liquid-Phase (SILP) Catalysis: Continuous-Flow Fixed-Bed Hydroformylation Of Propene. *Angew. Chem., Int. Ed.* **2005**, *44*, 815–819.
- (27) Wolf, P.; Aubermann, M.; Wolf, M.; Bauer, T.; Blaumeiser, D.; Stepic, R.; Wick, C. R.; Smith, D. M.; Smith, A. S.; Wasserscheid, P.; Libuda, J.; Haumann, M. Improving The Performance Of Supported Ionic Liquid Phase (SILP) Catalysts For The Ultra-Low-Temperature Water-Gas Shift Reaction Using Metal Salt Additives. *Green Chem.* **2019**, *21*, 5008–5018.
- (28) Lazzara, T. D.; Lau, K. K. H. A.; Abou-Kandil, A. I.; Caminade, A.; Majoral, P.; Knoll, W. Polyelectrolyte Layer-By-Layer. *ACS Appl. Mater. Interf.* **2010**, *4*, 3909–3920.
- (29) Roy, C. J.; Dupont-Gillain, C.; Demoustier-Champagne, S.; Jonas, A. M.; Landoulsi, J. Growth Mechanism Of Confined Polyelectrolyte Multilayers In Nanoporous Templates. *Langmuir* **2010**, *26*, 3350–3355.
- (30) Ali, M.; Yameen, B.; Cervera, J.; Ramírez, P.; Neumann, R.; Ensinger, W.; Knoll, W.; Azzaroni, O. Layer-By-Layer Assembly Of Polyelectrolytes Into Ionic Current Rectifying Solid-State Nanopores: Insights From Theory And Experiment. *J. Am. Chem. Soc.* **2010**, *132*, 8338–8348.
- (31) Derocher, J. P.; Mao, P.; Kim, J. Y.; Han, J.; Rubner, M. F.; Cohen, R. E. Layer-By-Layer Deposition Of All-Nanoparticle Multilayers In Confined Geometries. *ACS Appl. Mater. Interfaces* **2012**, *4*, 391–396.
- (32) Kim, J. Y.; Derocher, J. P.; Mao, P.; Han, J.; Cohen, R. E.; Rubner, M. F. Formation Of Nanoparticle-Containing Multilayers In Nanochannels Via Layer-By-Layer Assembly. *Chem. Mater.* **2010**, *22*, 6409–6415.
- (33) Dotzauer, D. M.; Bhattacharjee, S.; Wen, Y.; Bruening, M. L. Nanoparticle-Containing Membranes For The Catalytic Reduction Of Nitroaromatic Compounds. *Langmuir* **2009**, *25*, 1865–1871.
- (34) Xiao, F. Layer-By-Layer Self-Assembly Construction Of Highly Ordered Metal-TiO₂ Nanotube Arrays Heterostructures (M/Tnt_s, M = Au, Ag, Pt) With Tunable Catalytic Activities. *J. Phys. Chem. C* **2012**, *116*, 16487–16498.
- (35) Dotzauer, D. M.; Dai, J.; Sun, L.; Bruening, M. L. Catalytic Membranes Prepared Using Layer-By-Layer Adsorption Of Polyelectrolyte/Metal Nanoparticle Films In Porous Supports. *Nano Lett.* **2006**, *6*, 2268–2272.
- (36) Ouyang, L.; Dotzauer, D. M.; Hogg, S. R.; Macanás, J.; Lahitte, J. F.; Bruening, M. L. Catalytic Hollow Fiber Membranes Prepared Using Layer-By-Layer Adsorption Of Polyelectrolytes And Metal Nanoparticles. *Catal. Today* **2010**, *156*, 100–106.
- (37) Kanungo, S.; Paunovic, V.; Schouten, J. C.; Neira D'Angelo, M. F. Facile Synthesis Of Catalytic Aupd Nanoparticles Within Capillary Microreactors Using Polyelectrolyte Multilayers For The Direct Synthesis Of H₂O₂. *Nano Lett.* **2017**, *17*, 6481–6486.
- (38) Alem, H.; Blondeau, F.; Glinel, K.; Demoustier-Champagne, S.; Jonas, A. M. Layer-By-Layer Assembly Of Polyelectrolytes In Nanopores. *Macromolecules* **2007**, *40*, 3366–3372.
- (39) Derocher, J. P.; Mao, P.; Han, J.; Rubner, M. F.; Cohen, R. E. Layer-By-Layer Assembly Of Polyelectrolytes In Nanofluidic Devices. *Macromolecules* **2010**, *43*, 2430–2437.
- (40) Marinkovic, J. M.; Benders, S.; Garcia-Suarez, E. J.; Weiß, A.; Gundlach, C.; Haumann, M.; Küppers, M.; Blümich, B.; Fehrmann, R.; Riisager, A. Elucidating The Ionic Liquid Distribution In Monolithic SILP Hydroformylation Catalysts By Magnetic Resonance Imaging. *RSC Adv.* **2020**, *10*, 18487–18495.
- (41) Logemann, M.; Wolf, P.; Loipersböck, J.; Schrade, A.; Wessling, M.; Haumann, M. Ultra-Low Temperature Water–Gas Shift Reaction Catalyzed By Homogeneous Ru-Complexes In A Membrane Reactor – Membrane Development And Proof Of Concept. *Cat. Sci. Technol.* **2021**, *11*, 1558–1570.
- (42) Phillips, K. R.; England, G. T.; Sunny, S.; Shirman, E.; Shirman, T.; Vogel, N.; Aizenberg, J. A Colloidoscope Of Colloid-Based Porous Materials And Their Uses. *Chem. Soc. Rev.* **2016**, *45*, 281–322.
- (43) Stein, A.; Wilson, B. E.; Rudisill, S. G. Design And Functionality Of Colloidal–Crystal–Templated Materials—Chemical Applications Of Inverse Opals. *Chem. Soc. Rev.* **2013**, *42*, 2763–2803.
- (44) Aguirre, C. I.; Reguera, E.; Stein, A. Tunable Colors In Opals And Inverse Opal Photonic Crystals. *Adv. Funct. Mater.* **2010**, *20*, 2565–2578.
- (45) Hatton, B.; Mishchenko, L.; Davis, S.; Sandhage, K. H.; Aizenberg, J. Assembly Of Large-Area, Highly Ordered, Crack-Free Inverse Opal Films. *Proc. Natl. Acad. Sci. U. S. A.* **2010**, *107*, 10354–10359.
- (46) Logemann, M.; Marinkovic, J. M.; Schörner, M.; José García-Suárez, E.; Hecht, C.; Franke, R.; Wessling, M.; Riisager, A.; Fehrmann, R.; Haumann, M. Continuous Gas-Phase Hydroformylation Of But-1-Ene In A Membrane Reactor By Supported Liquid-Phase (SLP) Catalysis. *Green Chem.* **2020**, *22*, 5691–5700.
- (47) Giraudet, C.; Knoll, M. S. G.; Galvan, Y.; Süß, S.; Segets, D.; Vogel, N.; Rausch, M. H.; Fröba, A. P. Diffusion Of Gold Nanoparticles In Inverse Opals Probed By Heterodyne Dynamic Light Scattering. *Transp. Porous Media* **2020**, *131*, 723–737.
- (48) Raccis, R.; Nikoubashman, A.; Retsch, M.; Jonas, U.; Koynov, K.; Butt, H.-J.; Likos, C. N.; Fytas, G. Confined Diffusion In Periodic Porous Nanostructures. *ACS Nano* **2011**, *5*, 4607–4616.

(49) Schroden, R. C.; Al-Daous, M.; Blanford, C. F.; Stein, A. Optical Properties Of Inverse Opal Photonic Crystals. *Chem. Mater.* **2002**, *14*, 3305–3315.

(50) Burgess, I. B.; Koay, N.; Raymond, K. P.; Kolle, M.; Lončar, M.; Aizenberg, J. Wetting In Color: Colorimetric Differentiation Of Organic Liquids With High Selectivity. *ACS Nano* **2012**, *6*, 1427–1437.

(51) Zhang, S.; Vlémincq, C.; Ramirez Wong, D.; Magnin, D.; Glinel, K.; Demoustier-Champagne, S.; Jonas, A. M. Nanopapers Of Layer-By-Layer Nanotubes. *J. Mater. Chem. B* **2016**, *4*, 7651–7661.

(52) Butt, H.; Graf, K.; Kappl, M. *Physics And Chemistry Of Interfaces*; Wiley-VCH Verlag GmbH & Co. KGaA, 2003.

(53) Hunter, R. J. *Zeta Potential In Colloid Science*; Ottewill, R. H., Rowell, R., Eds.; Academic Press, 1981.

(54) Werner, S.; Szesni, N.; Bittermann, A.; Schneider, M. J.; Härter, P.; Haumann, M.; Wasserscheid, P. Screening Of Supported Ionic Liquid Phase (SILP) Catalysts For The Very Low Temperature Water-Gas-Shift Reaction. *Appl. Catal. Gen.* **2010**, *377*, 70–75.

(55) Werner, S.; Haumann, M.; Wasserscheid, P. Ionic Liquids In Chemical Engineering. *Annu. Rev. Chem. Biomol. Eng.* **2010**, *1*, 203–230.

(56) Wolf, P.; Logemann, M.; Schörner, M.; Keller, L.; Haumann, M.; Wessling, M. Multi-Walled Carbon Nanotube-Based Composite Materials As Catalyst Support For Water-Gas Shift And Hydroformylation Reactions. *RSC Adv.* **2019**, *9*, 27732–27742.

(57) Mehnert, C. P. Supported Ionic Liquid Catalysis. *Chem. - A Eur. J.* **2005**, *11*, 50–56.

(58) Steinrück, H.-P.; Wasserscheid, P. Ionic Liquids In Catalysis. *Catalysis Letters* **2015**, 380–397.

(59) Bauer, T.; Stepic, R.; Wolf, P.; Kollhoff, F.; Karawacka, W.; Wick, C. R.; Haumann, M.; Wasserscheid, P.; Smith, D. M.; Smith, A. S.; Libuda, J. Dynamic Equilibria In Supported Ionic Liquid Phase (SILP) Catalysis: In Situ IR Spectroscopy Identifies [Ru(CO)_xcly]_N Species In Water Gas Shift Catalysis. *Cat. Sci. Technol.* **2018**, *8*, 344–357.